Free Energy Principle for State and Input Estimation of a Quadcopter Flying in Wind

Bos, F.R.R.C.; Meera, Ajith Anil; Benders, Dennis; Wisse, Martijn

DOI
10.1109/ICRA46639.2022.9812415

Publication date
2022

Document Version
Final published version

Published in
Proceedings of the IEEE International Conference on Robotics and Automation, ICRA 2022

2022 IEEE International Conference on Robotics and Automation (ICRA)
May 23-27, 2022. Philadelphia, PA, USA

Free Energy Principle for State and Input Estimation of a Quadcopter Flying in Wind

Fred Bos [1], Ajith Anil Meera [2], Dennis Benders [3] and Martijn Wisse [4]

***Abstract*— The free energy principle from neuroscience provides a brain-inspired perception scheme through a data-driven model learning algorithm called Dynamic Expectation Maximization (DEM). This paper aims at introducing an experimental design to provide the first experimental confirmation of the usefulness of DEM as a state and input estimator for real robots. Through a series of quadcopter flight experiments under unmodelled wind dynamics, we prove that DEM can leverage the information from colored noise for accurate state and input estimation through the use of generalized coordinates. We demonstrate the superior performance of DEM for state estimation under colored noise with respect to other benchmarks like State Augmentation, SMIKF and Kalman Filtering through its minimal estimation error. We demonstrate the similarities in the performance of DEM and Unknown Input Observer (UIO) for input estimation. The paper concludes by showing the influence of prior beliefs in shaping the accuracy-complexity trade-off during DEM's estimation.**

I. INTRODUCTION

The widespread use of unmanned aerial vehicles (UAV) as delivery drones has increased the need for robust state and input estimators, mainly owing to its safety during uncertain events such as strong wind. We take a step in this direction by evaluating the usefulness of an approach from neuroscience to handle the wind during estimation.

In literature, a wide range of approaches have been used for the state estimation of linear time invariant (LTI) systems. However, most of them assume the noise to be white [1], which is often a wrong assumption in practice [2]. For example, Kalman filter (KF) [3] ensures optimality when the noises are white [4], but it is suboptimal when the noises are colored. An interesting approach from neuroscience called the Free Energy Principle (FEP) uses the concept called generalized coordinates that can leverage the noise derivative information in the brain signals for perception. The FEP based perception scheme called Dynamic Expectation Maximization (DEM) [5] was recently reformulated into a state and input observer for LTI systems with colored noise, and was shown to outperform the KF in simulation [6]. In this paper, we aim to provide the experimental validation of the DEM observer for a quadrotor under wind conditions using the setup given in Figure 1. The main contributions of the paper are:

1) Introduce an experimental design with real robots to provide the proof of concept for DEM as a state and input observer.
2) Provide the first experimental confirmation for the advantage of generalized coordinates in handling colored noise during state and input estimation on robots.
3) Demonstrate the influence of prior beliefs in shaping the accuracy-complexity trade-off during estimation.

All the authors are with the Cognitive Robotics department at TU Delft, The Netherlands. Corresponding author: ajitham1994@gmail.com.

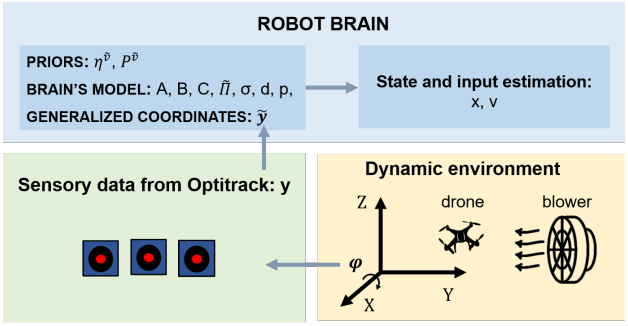

Fig. 1: The schematic representation of our experimental setup for the DEM's state and input estimation using a quadrotor.

II. RELATED WORK

This section introduces the interdisciplinary nature of FEP, connecting neuroscience and robotics.

A. Neuroscience

FEP emerges from neuroscience as a unified theory of the brain which posits that all biological systems resist their natural tendency to disorder by minimizing their free energy [7], where free energy is an information theoretic measure that bounds sensory surprisal. FEP provides a mathematical formalism for the brain related functions [8], unifies action and perception [9], connects memory and attention [8] and explains Freudian ideas [10]. The brain inspired nature of FEP has already attracted roboticists to apply it to build intelligent agents [11]. A few of them includes the body perception of humanoid robots [12], control of manipulator robot [13], system identification of a quadrotor [14, 15], SLAM [16], PID controller [17] etc. With this work we aim to assess the performance of DEM for state and input estimation of a quadrotor under wind conditions.

B. Robotics and control systems

In control systems literature, numerous approaches are used to deal with colored noise during state estimation. State Augmentation (SA) assumes the colored process noise as an auto-regressive (AR) noise and augments the state space equation to transform it into an equivalent system influenced by white noise [2]. The Measurement Differencing [18]

2022 IEEE International Conference on Robotics and Automation (ICRA) | 978-1-7281-9681-7/22/$31.00 ©2022 IEEE | DOI: 10.1109/ICRA46639.2022.9812415

approach deals with handling colored measurement noise. Second Moment Information Kalman filter (SMIKF) [19] extends KF for coloured noise by incorporating the temporal correlations of the AR noise into the prior covariance calculation of KF. In the fault detection literature, many observers have been developed for input estimation, like the Unknown Input Observer (UIO) [20]. However, none of these methods perform simultaneous state and input estimation under colored noise other than DEM [6].

In robotics, different approaches are used for state estimation of quadrotors under wind conditions. The most common approach (Dryden wind model) is to treat wind as a colored noise shaped by a filter acting on the white noise. Another approach is to model the wind dynamics and estimate wind velocity using complex nonlinear models [21]. Using additional cameras for accurate state estimation is another solution [22]. Our approach differs from these methods as we treat the wind noises as colored and use the information in the noise derivatives for accurate state and input estimation.

III. PROBLEM STATEMENT

Consider the plant dynamics given in Equation 1, where A, B and C are constant system matrices, $\mathbf{x} \in \mathbb{R}^n$ is the hidden state, $\mathbf{v} \in \mathbb{R}^r$ is the input and $\mathbf{y} \in \mathbb{R}^m$ is the output.

$$\dot{\mathbf{x}} = A\mathbf{x} + B\mathbf{v} + \mathbf{w}, \qquad \mathbf{y} = C\mathbf{x} + \mathbf{z}. \tag{1}$$

Here $\mathbf{w} \in \mathbb{R}^n$ and $\mathbf{z} \in \mathbb{R}^m$ are temporally correlated (colored) and represent the process and measurement noise respectively. The noises are assumed to be the result of the convolution of a Gaussian kernel on a white noise signal. The goal of the DEM observer is to simultaneously estimate $\mathbf{x}$ and $\mathbf{v}$, when the noises are colored (or non-white). The goal of this paper is to design an experimental setup for a real robot that can be used to validate the DEM observer and its usefulness in the presence of colored noise.

IV. PRELIMINARIES

This section introduces the DEM observer fundamentals.

A. Free energy principle

Fundamentally based on Bayesian Inference, FEP estimates the posterior probability $p(\vartheta/y) = p(\vartheta, y)/\int p(\vartheta, y)d\vartheta$, where ϑ is the component to be estimated and y is the measurement [23]. The presence of an intractable integral motivates the use of a variational density $q(\vartheta)$, called the recognition density that approximates the posterior as $q(\vartheta) \approx p(\vartheta/y)$. This approximation is achieved by minimizing the Kullback-Leibler (KL) divergence of the distributions given by $KL(q(\vartheta)||p(\vartheta/y)) = \langle \ln q(\vartheta) \rangle_{q(\vartheta)} - \langle \ln p(\vartheta/y) \rangle_{q(\vartheta)}$, where $\langle . \rangle_{q(\vartheta)}$ represents the expectation over $q(\vartheta)$. Upon simplification using $p(\vartheta/y) = p(\vartheta, y)/p(y)$, it can be rewritten as [7]:

$$\ln p(y) = F + KL(q(\vartheta)||p(\vartheta|y)), \tag{2}$$

where $F = \langle \ln p(\vartheta, y) \rangle_{q(\vartheta)} - \langle \ln q(\vartheta) \rangle_{q(\vartheta)}$ is the free energy. Since $\ln p(y)$ is independent of ϑ, minimization of the KL divergence involves the maximization of free energy. This is the fundamental idea behind using free energy as the proxy for brain's inference through the minimization of its sensory surprisal [7]. DEM uses this mathematical framework, in conjunction with the use of generalized coordinates to provide a hierarchical brain model [24]. We will be using a reformulated version of DEM given in [6] for this work.

B. Generative model

The key concept that differentiates DEM from other methods is its use of generalized coordinates for noise color handling. This is done by keeping track of the trajectory of all time-varying quantities (instead of only its point estimates) through a vector of derivatives. The state vector in generalized coordinates are written using a tilde operator as $\tilde{x} = [x \ x' \ x'' \ ....]^T$ where the dash operator represents the derivatives. Since the noises are colored, the higher derivatives of the system model can be written as [5]:

$$\begin{aligned} x' &= Ax + Bv + w & y &= Cx + z \\ x'' &= Ax' + Bv' + w' & y' &= Cx' + z' \\ &... & &... \end{aligned} \tag{3}$$

which can be compactly written as:

$$\dot{\tilde{x}} = D^x\tilde{x} = \tilde{A}\tilde{x} + \tilde{B}\tilde{v} + \tilde{w} \qquad \tilde{y} = \tilde{C}\tilde{x} + \tilde{z} \tag{4}$$

where $D^x = \begin{bmatrix} 0 & 1 & & \\ & 0 & 1 & \\ & & \ddots & \ddots \\ & & & 0 \end{bmatrix}_{(p+1)\times(p+1)} \otimes I_{n\times n}$.

Here, D^x represents the shift matrix, which performs the derivative operation on the generalized state vector. Similarly, D^v performs the same operation on inputs and has size $r(d+1)\times r(d+1)$. p and d represent the embedding order for the hidden states and the inputs respectively, indicating the number of derivatives used. The generalized system matrices are given by $\tilde{A} = I_{p+1} \otimes A$, $\tilde{B} = I_{p+1} \otimes B$, $\tilde{C} = I_{p+1} \otimes C$, where I denotes the identity matrix and $\otimes$ the Kronecker tensor product. The generalized output $\tilde{y}$ is calculated from the discrete measurements $\hat{y} = \begin{bmatrix} \cdots \\ y(t-dt) \\ y(t) \\ y(t+dt) \\ \cdots \end{bmatrix}_{m(p+1)}$ using the methodology in [5], resulting in a latency of $\frac{p}{2}dt$ during online estimation, which is negligible for the large sampling rate (120Hz) used in this paper.

C. Noise modeling

The use of generalized coordinates helps to model the noise color through the temporal precision matrix of the noise derivatives. In DEM, the noise is assumed to be the result of a white noise signal that has been convoluted using a Gaussian filter of the form: $K(t) = \frac{1}{\sqrt{2\pi}\sigma} exp(-\frac{1}{2}(\frac{t}{\sigma})^2)$. This provides an easy computation of the covariance of the noise derivatives using the temporal precision matrix S [5]:

$$S(\sigma^2) = \begin{bmatrix} 1 & 0 & -\frac{1}{2\sigma^2} & .. \\ 0 & \frac{1}{2\sigma^2} & 0 & .. \\ -\frac{1}{2\sigma^2} & 0 & \frac{3}{4\sigma^4} & .. \\ .. & .. & .. & .. \end{bmatrix}^{-1}_{(p+1)\times(p+1)} \tag{5}$$

σ is close to zero for white noise, while $\sigma > 0$ for colored noise. The generalized noise precision matrix can be written using S as $\tilde{\Pi} = diag(\tilde{\Pi}^z, P^{\tilde{v}}, \tilde{\Pi}^w)$, where $\tilde{\Pi}^z = S \otimes \Pi^z$, $\tilde{\Pi}^w = S \otimes \Pi^w$, and $P^{\tilde{v}} = S \otimes P^v$. Here Π^w and Π^z are the noise precisions (inverse covariance), and P^v is the prior precision on inputs.

D. State and Input Observer

The DEM observer in [6] simultaneously estimates the generalized state and input vector $X = \begin{bmatrix} \tilde{x} \\ \tilde{v} \end{bmatrix}$ through the gradient ascend over its variational free energy $V(t)$:

$$\dot{X} = kV(t)_X + D^X X, \tag{6}$$

where k is the learning rate, $V(t)_X$ is the gradient of $V(t)$ with respect to X and $D^X = \begin{bmatrix} D^x & O \\ O & D^v \end{bmatrix}$. Using the Laplace approximation [25], simplifies $V(t)$ as the precision weighted prediction error, $V(t) = -\frac{1}{2}\tilde{\epsilon}^T\tilde{\Pi}\tilde{\epsilon}$, where $\tilde{\epsilon}$ is the prediction error given by:

$$\tilde{\epsilon} = \begin{bmatrix} \tilde{y} - \tilde{C}\tilde{x} \\ \tilde{v} - \eta^{\tilde{v}} \\ D^x\tilde{x} - \tilde{A}\tilde{x} - \tilde{B}\tilde{v} \end{bmatrix} \tag{7}$$

Here $\eta^{\tilde{v}}$ denotes the prior on the input. Therefore, $V(t)_X = -\tilde{\epsilon}_X^T\tilde{\Pi}\tilde{\epsilon}$, where $\tilde{\epsilon}_X$ is given by:

$$\tilde{\epsilon}_X = \begin{bmatrix} -\tilde{C} & O \\ O & I \\ D^x - \tilde{A} & -\tilde{B} \end{bmatrix}. \tag{8}$$

Substituting these results to Equation 6 upon simplification yields the DEM state and input observer of [6]:

$$\dot{X} = \begin{bmatrix} \dot{\tilde{x}} \\ \dot{\tilde{v}} \end{bmatrix} = A_1 \begin{bmatrix} \tilde{x} \\ \tilde{v} \end{bmatrix} + B_1 \begin{bmatrix} \tilde{\mathbf{y}} \\ -\tilde{\eta} \end{bmatrix} \text{ and } Y = X, \tag{9}$$

where Y is the output of the observer, $A_1 = D^X - kA_2$,

$$A_2 = \begin{bmatrix} \tilde{C}^T\tilde{\Pi}^z\tilde{C} + (D^A)^T\tilde{\Pi}^w D^A & -(D^A)^T\tilde{\Pi}^w\tilde{B} \\ -\tilde{B}^T\tilde{\Pi}^w D^A & \tilde{P}^v + \tilde{B}^T\tilde{\Pi}^w\tilde{B} \end{bmatrix}, \tag{10}$$

$$B_1 = -\begin{bmatrix} -\tilde{C}^T\tilde{\Pi}^z & O \\ O & \tilde{P}^v \end{bmatrix} \text{ and } D^A = D^x - \tilde{A}.$$

This observer was proved to outperform the KF for state estimation on LTI systems with colored noise in simulation [6]. We will use an exact discretization of this observer throughout the paper to provide the experimental validation on a real robot.

E. Uncertainty in state and input estimation

DEM provides a means to compute the uncertainty in estimation through the precision of estimates given by the negative curvature of variational free energy [26]:

$$\Pi^X = -V(t)_{XX} = \tilde{\epsilon}_X^T\tilde{\Pi}\tilde{\epsilon}_X = A_2, \tag{11}$$

where A_2 is given in Equation 10. Therefore, the precision of DEM's state and input estimates is independent of time, and is given by $\Pi^{\tilde{x}\tilde{x}} = \tilde{C}^T\tilde{\Pi}^z\tilde{C} + (D^A)^T\tilde{\Pi}^w D^A$ and $\Pi^{\tilde{v}\tilde{v}} = \tilde{P}^v + \tilde{B}^T\tilde{\Pi}^w\tilde{B}$ respectively.

V. EXPERIMENTAL DESIGN

The distinctive feature of DEM that enables it to handle colored noise (to outperform a KF for state estimation) is its use of generalized coordinates [5, 6]. This section aims at designing an experimental setup (as simple as possible) for real robots that can leverage this property and provide a proof of concept for our DEM-based state and input observer design for LTI systems with colored noise [6].

A. Experimental setup

Our experimental setup consist of a quadrotor (Parrot AR.drone 2.0) hovering in wind produced by a blower in a controlled lab, as shown in Figure 2. The blower induces wind in the negative y direction, against the hovering quadcopter. We use an OptiTrack motion capture system to record the position and orientation of the quadcopter. The PID controller tries to resist the wind to hover the quadrotor at the given position $(0m, 0m, 1m)$ and orientation $(0°, 0°, 0°)$, using the onboard sensor data. A total of 9 hovering experiments were performed - 4 experiments without wind (blower off) and 4 experiments with wind (blower on). The final experiment was used to tune all the benchmark observers and will not be used for benchmarking. Each experiment lasted $10s$ with $dt = 0.0083s$. The Optitrack pose and PID control signals were recorded for offline evaluations.

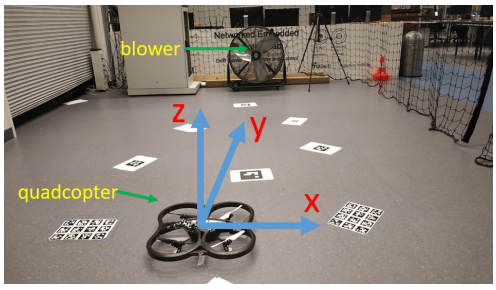

Fig. 2: The controlled lab environment for the experimental setup with the quadrotor and the blower.

Since wind is the result of another (unmodelled) dynamic system, we hypothesize that the introduction of wind influences the quadrotor dynamics and acts as the source of colored noise to the system. The experimental design enables us to control the level of noise color entering the system by controlling the blower for its wind speed and direction. We hypothesize that our DEM observer can leverage on the information contained in the colored noise by keeping track of the higher derivatives of states and inputs through the generalized coordinates.

B. Quadrotor model selection

The quadrotor model selection was performed to accommodate the influence of wind using minimum number of states, resulting in a controllable and observable LTI system. Since the wind flows in negative y direction, it influences the roll angle (ϕ around x-axis) and the roll angular velocity ($\dot{\phi}$) the most. Therefore, we only consider states $x = \begin{bmatrix} \phi \\ \dot{\phi} \end{bmatrix}$. The model involving these states is based on the one provided in

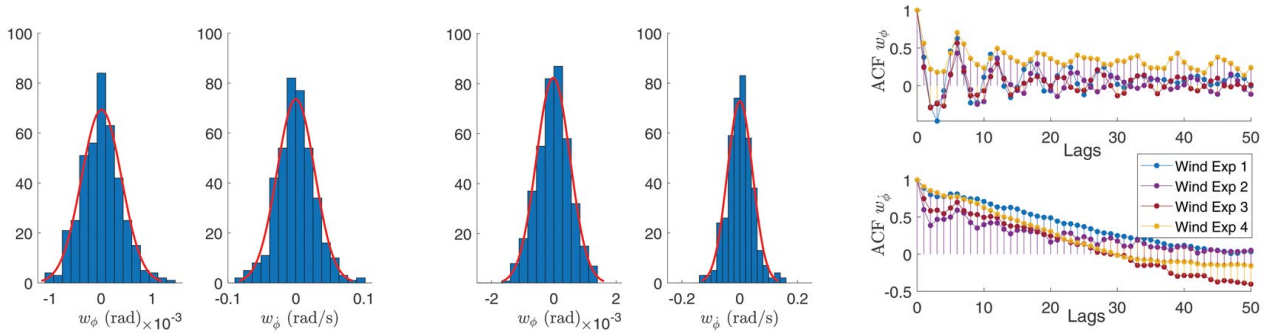

(a) Histograms of the process noise w_ϕ and $w_{\dot\phi}$ with a Gaussian fit for no wind conditions.

(b) Histograms of the process noise w_ϕ and $w_{\dot\phi}$ with a Gaussian fit under wind conditions.

(c) The auto-correlations for the process noises w_ϕ and $w_{\dot\phi}$ under wind conditions.

Fig. 3: The properties of process noise of our experiment. The wind introduces a colored Gaussian distributed disturbance to the system.

[27]. By assuming small angles, ϕ and $\dot{\phi}$ can be decoupled from the other system dynamics. Linearizing these states around hovering conditions gives:

$$\begin{bmatrix}\dot{\phi}\\ \ddot{\phi}\end{bmatrix} = \begin{bmatrix}0 & 1\\ 0 & 0\end{bmatrix}\begin{bmatrix}\phi\\ \dot{\phi}\end{bmatrix} + \begin{bmatrix}0 & 0 & 0 & 0\\ \frac{c_{B\phi}}{I_{xx}} & -\frac{c_{B\phi}}{I_{xx}} & -\frac{c_{B\phi}}{I_{xx}} & \frac{c_{B\phi}}{I_{xx}}\end{bmatrix}\begin{bmatrix}pwm_1\\ pwm_2\\ pwm_3\\ pwm_4\end{bmatrix}$$
$$y = \begin{bmatrix}1 & 0\end{bmatrix}\begin{bmatrix}\phi\\ \dot{\phi}\end{bmatrix} \tag{12}$$

Here pwm_i is the Pulse Width Modulation signal provided to the i^{th} motor by the controller for stable hovering. I_{xx} is the quadcopter's moment of inertia around the x-axis. It's value is identified using the bifilar pendulum experiment and equals $3.4 \cdot 10^{-3} kgm^2$. $c_{B\phi}$ is the thrust coefficient that models the relation between the PWM values and the thrust generated by the quadcopter rotors. It's value is obtained by averaging the results of several static thrust tests and equals $1.274 \cdot 10^{-3} Nm$. We normalize the input pwm signals using $v = \frac{v - mean(v)}{max(v) - min(v)}$ and use the same factor to multiply the B matrix, such that the system dynamics are unaltered. See [28] for more details regarding the model derivation, system identification procedure and experimental setup.

Since we use an accurate measurement system, Π^z is very high for all experiments. However, the presence of colored process noise w through wind makes $\Pi^w << \Pi^z$. Π^w is further influenced by the modelling errors during linearization as the wind aggressively drives the quadrotor away from its equilibrium.

VI. RESULTS AND ANALYSIS

This section aims to investigate the validity of the assumptions in our experimental design and to compare the performance of DEM observer against other benchmarks.

A. Validity of Laplace Approximation

The DEM framework approximates the probability densities of $p(\tilde{y})$ and $p(\tilde{x}/\tilde{v})$ to be Gaussian in nature, centred around their mean predictions ($\tilde{C}\tilde{x}$ and $\tilde{A}\tilde{x} + \tilde{B}\tilde{v}$, respectively) with the same precision as that of the noises ($\tilde{\Pi}^z$ and $\tilde{\Pi}^w$):

$$p(\tilde{y}) = \frac{1}{\sqrt{(2\pi)^{m(p+1)}|\tilde{\Sigma}^z|}} e^{-\frac{1}{2}(\tilde{y}-\tilde{C}\tilde{x})^T \tilde{\Pi}^z (\tilde{y}-\tilde{C}\tilde{x})},$$
$$p(\tilde{x}/\tilde{v}) = \frac{1}{\sqrt{(2\pi)^{n(p+1)}|\tilde{\Sigma}^w|}} e^{-\frac{1}{2}\tilde{\epsilon}^{xT}\tilde{\Pi}^w\tilde{\epsilon}^x}, \tag{13}$$

where $\tilde{\epsilon}^x = D^x\tilde{x} - \tilde{A}\tilde{x} - \tilde{B}\tilde{v}$. The validity of this approximation on our experimental design was investigated by plotting the process noise histograms for both without wind and with wind conditions (for 400 data points each) and is shown in Figure 3a and 3b respectively. Similar trend holds for measurement noise as well. The strong Gaussian fit indicates the validity of Laplace approximation for our experimental design.

B. Influence of wind on states and process noise

In this section we validate the direct influence of wind on the states and process noise. Table I demonstrates a higher standard deviation for windy conditions than for non-windy conditions. A similar trend can be observed from the width of histograms in Figure 3a and 3b, indicating that our experimental design can control the noise generation.

	ϕ (rad)	$\dot{\phi}$ (rad/s)	w_ϕ (rad)	$w_{\dot\phi}$ (rad/s)
Without wind	0.00855	0.0544	0.000416	0.0284
With wind	0.0460	0.260	0.000937	0.0607

TABLE I: The standard deviations of the states, ϕ and $\dot{\phi}$, and the process noises, w_ϕ and $w_{\dot\phi}$, for experiments with and without wind.

C. Confirmation of noise color

In this section we confirm that our experimental design generates colored process noise. Figure 3c shows the sample auto-correlation of the process noise of all experiments (with wind). There is stronger autocorrelation for $w_{\dot\phi}$ than for w_ϕ, because ϕ is observed. The auto-correlation is different from that expected from a white noise signal where the auto-correlation immediately drops to 0 after zero lag. This confirms the presence of strong noise color (time-correlated noise) in data.

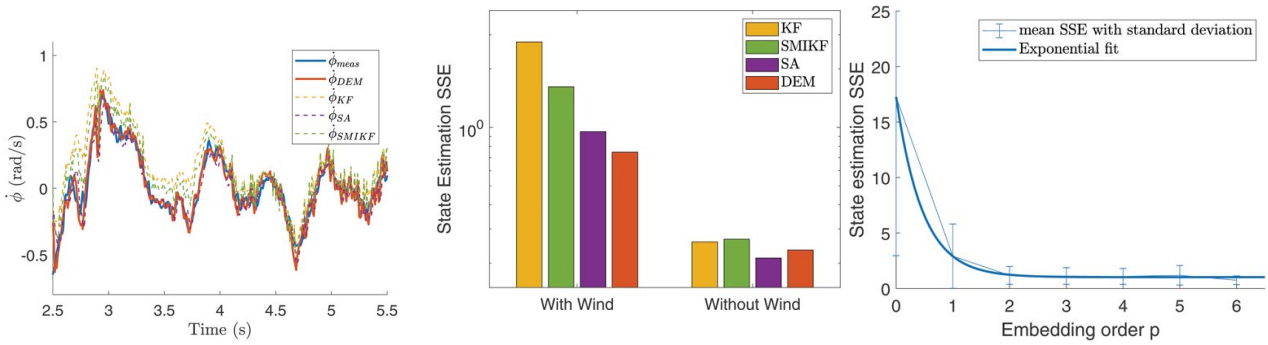

(a) State estimation benchmarks with wind. (b) Average SSE of all flights. (c) Average SSE drops exponentially with p.

Fig. 4: DEM outperforms other benchmarks with minimal SSE in state estimation for a quadrotor flying under windy conditions. The performance of DEM improves exponentially with higher orders of generalized motion p, for a quadrotor flying under windy conditions, highlighting the importance of generalized coordinates in the presence of colored noise.

D. Estimator settings for benchmarking

We aim to benchmark the state estimation against KF, SMIKF and SA, and the input estimation against UIO, for a total of 8 experiments (4 with and 4 without wind). All methods use the same data $\mathbf{y}$ and initial condition $x(0) = \left[\begin{smallmatrix}0\\0\end{smallmatrix}\right]$. DEM was set with learning rate $k = 1$, and the order of generalized motion of states and inputs to $p = 6$ and $d = 2$ respectively. The SMIKF implementation could only accommodate a first order AR model, while the SA implementation uses a 6^{th} order AR model, similar to the 6^{th} order derivatives (p) of DEM. The noise precision Π^w was calculated for each experiment, while $\Pi^z = 8.1 \cdot 10^{-9}$ was calculated from static drone data. The 9^{th} experiment was used to tune the noise smoothness to $\sigma = 0.006$, which was used for all experiments. The computational complexities of SMIKF, SA and DEM are theoretically higher than KF.

E. State estimation - benchmarking

In this section, we compare the performance of DEM with the aforementioned benchmarks for state estimation with known inputs. Figure 4a shows the state estimates of all benchmarks for an experiment with wind (zoomed for visualization). Although most benchmarks follow the general trend of the measured states (in blue), DEM performs the best. KF shows an inferior performance due to its incapability of dealing with colored noise. We use the sum of squared errors (SSE) between the estimate of $\dot{\phi}$ and its measurement as the metric to denote the quality of state estimation. The average SSE of all 4 experiments (with and without wind separately) for all benchmarks are shown in Figure 4b. DEM outperforms other benchmarks in state estimation under wind conditions with minimal SSE, demonstrating that it is a competitive state estimator.

F. Role of Generalized Coordinates

One of the main strengths of DEM - the capability to deal with colored noise - comes from the use of generalized coordinates. In this section, we demonstrate the usefulness of generalized coordinates in state estimation on experimental data. The mean (and standard deviations of) SSE of state estimation for all experiments (with wind) for varying orders of generalized motion p is shown in Figure 4c. The exponential decrease in SSE is consistent with the results from [6] on large simulated data, and indicates the importance of generalized coordinates in accurate state estimation in the presence of colored noise.

G. State estimation as free energy maximization

The fundamental idea behind state estimation using DEM is the gradient ascent over the variational free energy manifold. In this section, we visually demonstrate that DEM's state estimates for flight experiment maximize $V(t)$. Figure 5 shows that the DEM state estimate is on top of the $V(t)$ curve at each time instance.

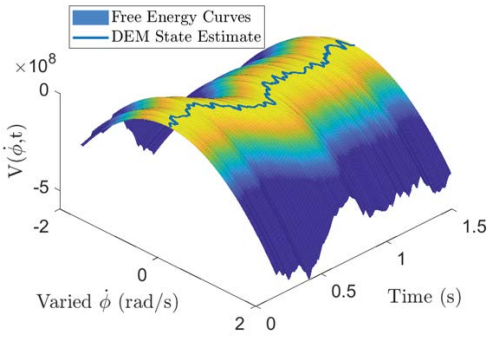

Fig. 5: The DEM state estimate (blue curve) lies on top of the variational free energy surface, indicating that the DEM observer maximized $V(t)$. Plot zoomed for visualization.

H. Input Estimation - benchmarking

In this section, we aim to demonstrate our DEM observer's capability to estimate inputs in real robot application and benchmark it against an input observer (UIO) from control systems. We use the same settings as given in Section VI-D, except for providing the input priors for pwm_1 with a wrong value of $\eta^{pwm_1} = 0.5$ with a low precision of $P^{pwm_1} = 1$ to encourage exploration and $\Pi^w = e^3 I_2$. We use $C = I$ for this section to meet the observability requirements of our

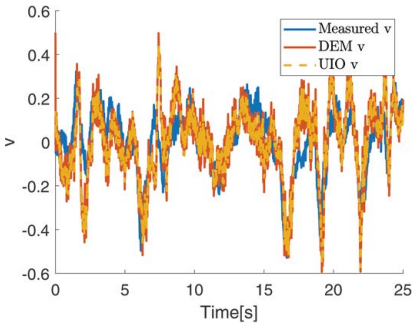

Fig. 6: DEM's input estimation coinciding with that of UIO.

benchmark (UIO). Both DEM and UIO estimated the first pwm signal and the result is shown in Figure 6. Both DEM and UIO followed the trend of measured inputs (in blue).

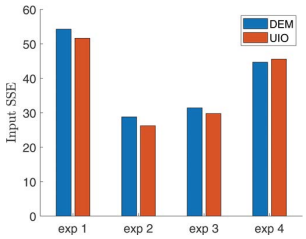

Fig. 7: Similar performance of DEM and UIO for input estimation indicated by similar SSE in input estimation.

The coinciding input estimates for DEM and UIO demonstrate that both estimators behave the same. The estimation was repeated for all experiments and the SSE for input estimation is shown in Figure 7. This confirms the similarity in performance of UIO and DEM for input estimation in the presence of colored noise.

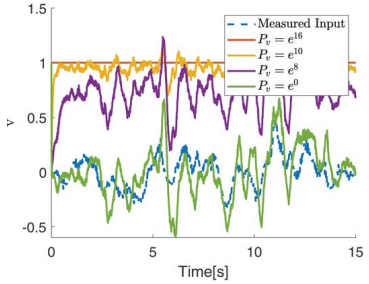

Fig. 8: The input estimates moving from a wrong prior of $\eta^v = 1$ to the measured input (in blue), mediated by the prior precision P_v.

I. Accuracy v/s complexity

The inherent capability of DEM to balance between estimation accuracy and complexity is mediated by the priors η^v and P^v [6]. Here, accuracy is the measure of closeness of estimates to the real measurement, and complexity is the measure of closeness to the priors. This section aims at demonstrating this balance for simultaneous state and input estimation on quadrotor data. This section follows the same settings as Section VI-D with $\Pi^w = e^3 I_2$. Simultaneous state and input estimation was performed using wrong input prior $\eta^v = 1$ for varying prior precisions P^v, and the resulting input estimation is shown in Figure 8, along with the measured input (in blue). As P^v is relaxed, the input estimation moves away from the wrong prior η^v and moves closer to the correct inputs. The shift from wrong priors to the correct measurements, mediated by P^v can be seen as a balance (trade-off) between complexity and accuracy. Figure 9 demonstrates this balance for all experiments with windy conditions, both for state and input estimation. The increasing SSE for higher P^v indicates the shift from high accuracy with low complexity region to the low accuracy with high complexity region. This trade-off is useful mainly in industrial fault detection systems where any major deviations from the prior (known) inputs could be detected and isolated during runtime. DEM's inherent capability to balance accuracy and complexity is an added advantage when compared to other input estimators in literature like UIO.

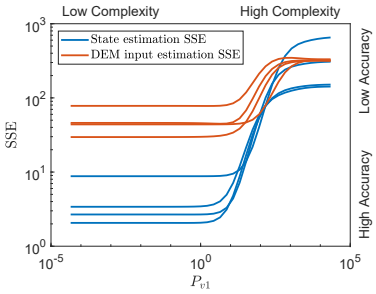

Fig. 9: The SSE plot of state and input estimation demonstrating DEM's accuracy-complexity tradeoff. The SSE moves from a region of low complexity and high accuracy to a region of high complexity and low accuracy as the prior precision P^v is increased.

VII. CONCLUSIONS AND FUTURE WORK

The FEP based perception scheme called DEM, has recently been reformulated into a simulataneous state and input observer for LTI systems under colored noise. With this paper, we propose an experimental design to validate the DEM observer on real robots. Through a series of quadrotor experiments under wind conditions, we show that the DEM based observer outperforms other benchmarks like KF, SMIKF and SA for state estimation with minimum estimation errors. We show that DEM's input estimation shows similar performance compared to classical input observers like UIO. With this paper, we provide the first experimental validation for the use of generalized coordinates to deal with colored noise during state and input estimation on real robots. We further demonstrate the unique capability of DEM to balance between accuracy and complexity during state and input estimation. The main challenge of the DEM observer is the need to know the noise precision and noise smoothness *a priori*. We intend to extend this work for simultaneous noise precision and smoothness estimation in future.

VIII. ACKNOWLEDGEMENT

We would like to thank Prof. Tamás Keviczky for letting us use the lab facilities in the midst of corona crisis.

REFERENCES

[1] A. C. Jalfon and Y. Halevi, "On partially augmented observers for systems with coloured noises," *International Journal of Control*, vol. 57, no. 2, pp. 335–349, 1993.

[2] A. Bryson and D. Johansen, "Linear filtering for time-varying systems using measurements containing colored noise," *IEEE Transactions on Automatic Control*, vol. 10, no. 1, pp. 4–10, 1965.

[3] B. P. Gibbs, *Advanced Kalman filtering, least-squares and modeling: a practical handbook*. John Wiley & Sons, 2011.

[4] R. E. Kalman, "A new approach to linear filtering and prediction problems," *Transactions of the ASME–Journal of Basic Engineering*, vol. 82, no. Series D, pp. 35–45, 1960.

[5] K. J. Friston, N. Trujillo-Barreto, and J. Daunizeau, "Dem: a variational treatment of dynamic systems," *Neuroimage*, vol. 41, no. 3, pp. 849–885, 2008.

[6] A. A. Meera and M. Wisse, "Free energy principle based state and input observer design for linear systems with colored noise," in *2020 American Control Conference (ACC)*. IEEE, 2020, pp. 5052–5058.

[7] K. Friston, "The free-energy principle: a unified brain theory?" *Nature reviews neuroscience*, vol. 11, no. 2, pp. 127–138, 2010.

[8] ——, "The free-energy principle: a rough guide to the brain?" *Trends in cognitive sciences*, vol. 13, no. 7, pp. 293–301, 2009.

[9] K. J. Friston, J. Daunizeau, J. Kilner, and S. J. Kiebel, "Action and behavior: a free-energy formulation," *Biological cybernetics*, vol. 102, no. 3, pp. 227–260, 2010.

[10] R. L. Carhart-Harris and K. J. Friston, "The default-mode, ego-functions and free-energy: a neurobiological account of freudian ideas," *Brain*, vol. 133, no. 4, pp. 1265–1283, 2010.

[11] P. Lanillos, C. Meo, C. Pezzato, A. A. Meera, M. Baioumy, W. Ohata, A. Tschantz, B. Millidge, M. Wisse, C. L. Buckley *et al.*, "Active inference in robotics and artificial agents: Survey and challenges," *arXiv preprint arXiv:2112.01871*, 2021.

[12] G. Oliver, P. Lanillos, and G. Cheng, "Active inference body perception and action for humanoid robots," *arXiv preprint arXiv:1906.03022*, 2019.

[13] C. Pezzato, R. Ferrari, and C. H. Corbato, "A novel adaptive controller for robot manipulators based on active inference," *IEEE Robotics and Automation Letters*, vol. 5, no. 2, pp. 2973–2980, 2020.

[14] A. Anil Meera and M. Wisse, "A brain inspired learning algorithm for the perception of a quadrotor in wind," *arXiv preprint arXiv:2109.11971*, 2021.

[15] ——, "On the convergence of dem's linear parameter estimator," in *Machine Learning and Principles and Practice of Knowledge Discovery in Databases*. Cham: Springer International Publishing, 2021, pp. 692–700.

[16] O. Çatal, T. Verbelen, T. Van de Maele, B. Dhoedt, and A. Safron, "Robot navigation as hierarchical active inference," *Neural Networks*, vol. 142, pp. 192–204, 2021.

[17] M. Baltieri and C. L. Buckley, "Pid control as a process of active inference with linear generative models," *Entropy*, vol. 21, no. 3, p. 257, 2019.

[18] A. Bryson Jr and L. Henrikson, "Estimation using sampled data containing sequentially correlated noise." *Journal of Spacecraft and Rockets*, vol. 5, no. 6, pp. 662–665, 1968.

[19] Z. Zhou, J. Wu, Y. Li, C. Fu, and H. Fourati, "Critical issues on kalman filter with colored and correlated system noises," *Asian Journal of Control*, vol. 19, no. 6, pp. 1905–1919, 2017.

[20] B. A. Charandabi and H. J. Marquez, "Observer design for discrete-time linear systems with unknown disturbances," in *2012 IEEE 51st IEEE Conference on Decision and Control (CDC)*. IEEE, 2012, pp. 2563–2568.

[21] S. Waslander and C. Wang, "Wind disturbance estimation and rejection for quadrotor position control," in *AIAA Infotech@ Aerospace conference and AIAA unmanned... Unlimited conference*, 2009, p. 1983.

[22] D. Abeywardena, Z. Wang, G. Dissanayake, S. L. Waslander, and S. Kodagoda, "Model-aided state estimation for quadrotor micro air vehicles amidst wind disturbances," in *2014 IEEE/RSJ International Conference on Intelligent Robots and Systems*. IEEE, 2014, pp. 4813–4818.

[23] C. L. Buckley, C. S. Kim, S. McGregor, and A. K. Seth, "The free energy principle for action and perception: A mathematical review," *Journal of Mathematical Psychology*, vol. 81, pp. 55–79, 2017.

[24] K. Friston, "Hierarchical models in the brain," *PLoS computational biology*, vol. 4, no. 11, p. e1000211, 2008.

[25] K. Friston, J. Mattout, N. Trujillo-Barreto, J. Ashburner, and W. Penny, "Variational free energy and the laplace approximation," *Neuroimage*, vol. 34, no. 1, pp. 220–234, 2007.

[26] A. Anil Meera and M. Wisse, "Dynamic expectation maximization algorithm for estimation of linear systems with colored noise," *Entropy*, vol. 23, no. 10, p. 1306, 2021.

[27] S. Bouabdallah, P. Murrieri, and R. Siegwart, "Design and control of an indoor micro quadrotor," in *IEEE International Conference on Robotics and Automation, 2004. Proceedings. ICRA '04. 2004*, vol. 5, 2004, pp. 4393–4398 Vol.5.

[28] D. Benders, "Ar.drone 2.0 state estimation using dynamic expectation maximization," Master's thesis, 2020, available at http://resolver.tudelft.nl/uuid:156157c6-d7f0-4dc1-a55a-b2e4ed66f1c2.